Numerical simulations of the guided elastic waves generated by laser-induced AS and ES in hollow cylinders*

TANG Liguo and CHENG Jianchun**

(The National Laboratory of Acoustics, Nanjing University, Nanjing 210093, China)

Received August 14, 2002; revised September 18, 2002

Abstract Numerical analyses are presented for the laser-generated guided elastic waves in hollow cylinders. The transient waveforms excited by the ablation source (AS) and the evaporation source (ES), due to the ablation and the evaporation of oil induced by impinging laser pulse, are calculated numerically by modeling different time-dependencies, i.e. the former is considered as Heaviside step function and the latter is assumed to be Dirac Delta function. Instead of using classical integral transform, the method of eigen-function expansion is employed, by which time-dependent displacement at the outer surface of hollow cylinders will be expressed by summation of longitudinal and flexural type modes. This formula is particularly suitable for analyses of generation efficiency of each guided elastic mode. And the waveform of total radial displacements were analyzed using a short-time Fourier transform (STFT).

Keywords: eigen-function, guided elastic wave, longitudinal, flexural, evaporation source, ablation source.

Corrosion and pitting defects in pipe-work are major problems in the oil, gas, chemical and other industries. They may lead to serious consequences if they would not be detected in time. In order to inspect the tube efficiently, many researchers are exploring the use of ultrasonic guided waves for pipe inspection[1~8]. However, ultrasonic guided wave propagation and reflection in tubing is still not completely understood. The first exact and complete solution of the problem of time harmonic waves in a hollow cylinder satisfying traction free boundary conditions on its lateral boundaries was presented by Gazis[9] using elasticity theory in 1959. For the generation of ultrasonic guided waves in heat exchanger tubing, Silk and Bainton[1] investigated piezoelectric ultrasonic probes to access the inside of the tube. Their objective was mainly to generate and use the L(0, 1) mode. But Alleyne et al.[2,3] suggested the use of the L(0, 2) mode, which is the fastest mode in a non-dispersive region of frequency range to minimize dispersion effects over long distances. Recently, Li and Rose[6,7] studied excitation and propagation of non-axisymmetric guided waves in a hollow cylinder by using the normal mode expansion method, i.e. eigen-function expansion method, and their researches focused on the variance of angular profiles for different propagating distance of the guided wave excited by non-axisymmetric partial loading such as an angle beam source. We[8] have studied the influence of the spatial distribution of laser beams to the generation of guided waves in a hollow cylinder and given the numerical simulations of the propagation of guided waves when the laser beams beat on the outer surface of a hollow cylinder axisymmetrically. In addition, the research of using the non-axisymmetric modes for pipe inspection is in progress[5].

Up to now, ultrasonic guided waves are mainly excited and received by piezoelectric transducers for pipe inspection. However, this method of contact sometimes may be inconvenient in practical situations such as inspection of on-line chemical pipe. Therefore, it is necessary to develop and apply non-contact methods, such as electromagnetic acoustic transducers (EMAT)[10,11] and laser ultrasonic technique[12,13]. Our work is focused on laser-generated guided wave in hollow cylinders for pipe inspection. However, a main disadvantage of laser-generated ultrasonic testing is that multiple guided modes can be excited at the same time by the laser pulse. Due to dispersion of guided waves, the waveforms will be distorted in space and in time. This complicates analysis of the waveforms in the process of detection. Even though, this complexity makes recognition of some type of defects impossible. Therefore, it is necessary to clarify dynamic response to the laser pulses for generation of

* Supported by the Doctoral Foundation of Education Ministry of China (No. 1999028432) and the National Natural Science Foundation of China (Grant No. 19974017)

** To whom correspondence should be addressed. E-mail: jccheng@nju.edu.cn

ultrasonic guided waves.

In this paper, we present numerical simulations for guided waves generated by impinging laser pulse in a hollow cylinder. The laser pulse is assumed to be radial incident on outer surface of the hollow cylinder. The transient waveforms excited from different acoustic sources, due to the ablation and the evaporation of oil induced by laser pulse, are calculated numerically by modeling different time-dependencies, i. e. the former is considered as Heaviside step function and the latter is assumed to be Dirac Delta function. On the other hand, instead of using classical integral transform techniques to solve the transient problem, the method of eigen-function expansion is employed, by which the time-dependent radial displacement at the outer surface of hollow cylinders will be expressed by summation of longitudinal and flexural type modes. This formula is particularly suitable for analyses of generation efficiency of each guided elastic mode. At last, the waveforms of total radial displacements were analyzed using a short-time Fourier transform(STFT) and the plots of time-frequency analysis were given.

1 Elastodynamics theory in hollow cylinders

The motion of an isotropic, homogeneous elastic body with externally applied force density $\boldsymbol{f}(\boldsymbol{r}, t)$ in the body V and force density $\boldsymbol{s}(\boldsymbol{r}, t)$ at the surface Σ, respectively, is governed by elastodynamic equation

$$\boldsymbol{L}(\boldsymbol{u}) \equiv (\lambda + \mu)\nabla(\nabla \cdot \boldsymbol{u}) + \mu \nabla^2 \boldsymbol{u} = \rho \frac{\partial^2 \boldsymbol{u}}{\partial t^2} - \rho \boldsymbol{f}(\boldsymbol{r}, t), \quad \boldsymbol{r} \in V, \tag{1a}$$

with the boundary condition

$$\boldsymbol{B}(\boldsymbol{u}) \equiv (\lambda(\nabla \boldsymbol{u}) + \mu[\nabla \boldsymbol{u} + (\nabla \boldsymbol{u})^{\mathrm{T}}]) \cdot \boldsymbol{n} = \boldsymbol{s}(\boldsymbol{r}, t), \quad \boldsymbol{r} \in \Sigma, \tag{1b}$$

where λ and μ are the Lamé constants of the material, $\boldsymbol{u}(\boldsymbol{r}, t)$ is displacement field vector and the superscript T indicates the transposition of a tensor. Before considering the case of forced motion, we discuss first the free vibration of a hollow cylinder with $\boldsymbol{f}(\boldsymbol{r}, t) = 0$ in Eq. (1) with the stress-free boundary conditions at the outer and inner surfaces

$$\sigma_{rr}\Big|_{r=a,b} = 0, \quad \sigma_{r\theta}\Big|_{r=a,b} = 0, \quad \sigma_{rz}\Big|_{r=a,b} = 0, \tag{2a}$$

where a and b are the inner and outer radii, respectively, as shown in Fig. 1. If the length of the hollow cylinder is $2l$ and rigid-smooth boundary conditions are applied to the surfaces $z = \pm l$, one has

$$u_z\Big|_{z=\pm l} = 0, \quad \sigma_{zr}\Big|_{z=\pm l} = 0, \quad \sigma_{z\theta}\Big|_{z=\pm l} = 0. \tag{2b}$$

Note that it is not possible to obtain an analytical solution for the eigen-value problem[14] if the traction-free or rigid boundary conditions are employed. If the hollow cylinder is long enough or the detection spot is far from the boundary, the effect of the boundary conditions on propagation of the guided waves is negligible, which has been proven in our numerical analyses. If scattering of the boundary is considered, one has to take a real boundary condition. In addition to these boundary conditions, there are also the initial conditions

$$\boldsymbol{u}(\boldsymbol{r}, t) = 0, \quad \frac{\partial \boldsymbol{u}(\boldsymbol{r}, t)}{\partial t} = 0 \quad \text{for} \quad t \leqslant 0. \tag{3}$$

This problem has been exhaustively examined in Ref. [9] and three classes of guided wave modes propagating in hollow cylinders: (1) the longitudinal axially symmetric modes, L(0, m) (m = 1, 2, 3, 4, ⋯); (2) the torsional axially symmetric modes, T(0, m) (m = 1, 2, 3, 4, ⋯); and (3) the flexural non-axially symmetric modes, F(n, m) (n, m = 1, 2, 3, 4, ⋯). The group velocity curves of the first six branches of L(0, m) and F(1, m) are shown in Fig. 2. The values of the geometry and material

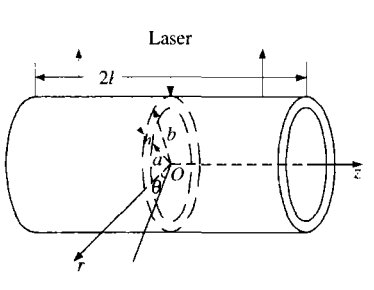

Fig. 1. A hollow cylinder with outer radius b, wall thickness h, and length $2l$.

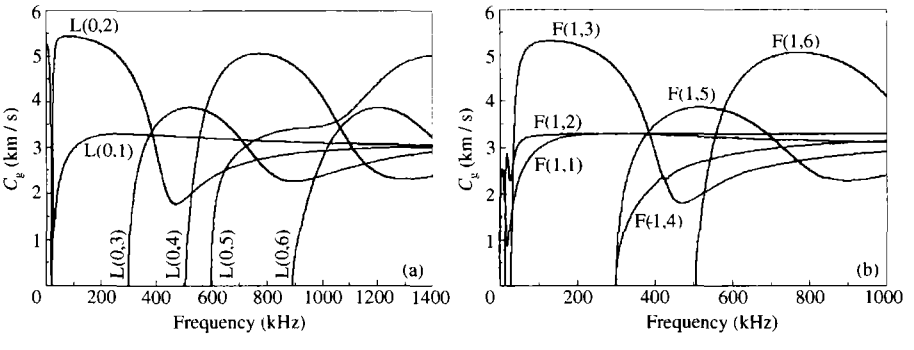

Fig. 2. The group velocity curves of first six branches of L(0, m) and F(1, m) with OD = 88.7 mm and the wall thickness h = 5.5 mm.

parameters used in all numerical simulations are the thickness $h = 5.5$ mm, OD = 88.7 mm, the Poisson's ratio $\gamma = 0.28$, the Lamé constant $\mu = 8.4$ GPa and the density $\rho = 7.8 \times 10^3$ kg/m^3.

For a finite length hollow cylinder, the wave-number ξ in the z-direction is restricted to a set of discrete real irrational numbers,

$$\xi_k = k\pi/l \quad (k = 1, 2, 3, \cdots). \tag{4}$$

There exist infinite values of eigen-frequency ω_{nmk} for each value of ξ_k, which is decided by the dispersive equation. Note that the mode designation in this paper follows the notations used by Meitzler[15] and Zemannek[16], which appears to be used as a standard system in the literature.

2 Eigen-function expansion

The eigen-value problem of the linear differential operator $\boldsymbol{L}$ is defined by

$$\boldsymbol{L}[\boldsymbol{u}_{nmk}] = -\rho\omega_{nmk}^2\boldsymbol{u}_{nmk}, \quad \boldsymbol{r} \in V, \tag{5a}$$

$$\boldsymbol{B}[\boldsymbol{u}_{nmk}] = 0, \quad \boldsymbol{r} \in \Sigma. \tag{5b}$$

It has been shown that the eigen-values are real and non-negative[17]. Furthermore, the linear differential operator $\boldsymbol{L}$ is self-adjoint under the boundary operator $\boldsymbol{B}$[14,18]. Therefore, the eigenfunctions $\boldsymbol{u}_{nmk}$ form an orthogonal set, i.e.

$$\int_V \rho\boldsymbol{u}_{nmk}\cdot\boldsymbol{u}_{pqj}\,\mathrm{d}V = \begin{cases} 0, & n \neq p \text{ or } m \neq q \text{ or } k \neq j \\ M_{nmk}, & n = p,\ m = q \text{ and } k \neq j \end{cases} \tag{6a}$$

where M_{nmk} is the norm of $\boldsymbol{u}_{nmk}$

$$M_{nmk} = \int_{-l}^{l}\int_a^b\int_0^{2\pi} \rho\boldsymbol{u}_{nmk}(r,\theta,z)\cdot\boldsymbol{u}_{nmk}(r,\theta,z)\,r\,\mathrm{d}r\,\mathrm{d}\theta\,\mathrm{d}z. \tag{6b}$$

The eigen-function corresponding to the wave-number ξ_k and eigen-frequency ω_{nmk} is

$$\boldsymbol{u}_{nmk}(r,\theta,z) = u_{nmk}^r(r,\theta,z)\boldsymbol{e}_r + u_{nmk}^\theta(r,\theta,z)\boldsymbol{e}_\theta + u_{nmk}^z(r,\theta,z)\boldsymbol{e}_z, \tag{7a}$$

where

$$u_{nmk}^r(r,\theta,z) = R_{nmk}^r(r,\xi_k,\omega_{nmk})\cos n\theta\cos\xi_k z, \tag{7b}$$

$$u_{nmk}^\theta(r,\theta,z) = R_{nmk}^\theta(r,\xi_k,\omega_{nmk})\sin n\theta\cos\xi_k z, \tag{7c}$$

$$u_{nmk}^z(r,\theta,z) = R_{nmk}^z(r,\xi_k,\omega_{nmk})\cos n\theta\sin\xi_k z. \tag{7d}$$

Hence the solution of non-homogeneous Eq. (1) can be expanded by eigen-function series

$$\boldsymbol{u}(r,\theta,z,t) = \sum_{nmk} q_{nmk}(t)\boldsymbol{u}_{nmk}(r,\theta,z), \tag{8a}$$

where

$$q_{nmk}(t) = \frac{1}{M_{nmk}\omega_{nmk}}\int_0^t \Phi_{nmk}(\tau)\sin\omega_{nmk}(t-\tau)\,\mathrm{d}\tau, \tag{8b}$$

$$\Phi_{nmk}(t) = \int_V \boldsymbol{f}(\boldsymbol{r},t)\cdot\boldsymbol{u}_{nmk}(\boldsymbol{r})\,\mathrm{d}V + \int_S \boldsymbol{s}(\boldsymbol{r},t)\cdot\boldsymbol{u}_{nmk}(\boldsymbol{r})\,\mathrm{d}S. \tag{8c}$$

Generally, two methods, the integral transform and the eigen-function expansion, are used to study the transient motion of an elastic body in elastodynamics. Compared with the former, the latter is more suitable to study the guided waves in thin plates[19] and hollow cylinders. The transient displacement field $\boldsymbol{u}(\boldsymbol{r},t)$ is simply the summation of several lower guided modes, if only several guided wave modes will be excited in thin plates and tubes.

3 Laser-generated guided waves

In detection of metal tubes by laser-based ultrasound, the laser beam can be focused to sufficiently high power densities at the metal surface so that material ablation and subsequent plasma formation are caused. Hutchins et al.[12,13] have discussed the mechanism of acoustic generation from ablation and plasma formation. The ablation source (AS) is dominated by a normal force mono-pole with a time dependence that approximates to a Heaviside step function $H(t)$. For non-destructive detection, a thin coating of oil at the generation spot can be added to increase the acoustic generation efficiency from the laser pulse with lower power densities. In this case, evaporation of the oil becomes dominant sources. The generation mechanism of acoustic sources by evaporation of the oil is that momentum is transferred from the evaporating particles to the solid surface. The evaporating source (ES) is dominated by a normal mono-pole force with a time dependence of Dirac Delta function $\delta(t)$[12,13]. Under the above two cases, the acoustic source can be considered to be located at the surface with the bulk force density $\boldsymbol{f} = 0$ and the surface force density $\boldsymbol{s}$ is radial force.

Note that the Dirac Delta function is the derivative of the Heaviside step function, so that the waveform generated by the ES is the derivative of that generated by the AS. For simplicity, we presume that the laser pulse has a Gaussian distribution along

axis z with the spot radius d and the center of the laser spot is located at $z=0$.

Based on analyses above, the surface force induced by the AS can be shown as

$$\boldsymbol{s}(r,\theta,z,t)\Big|_{r=b}=b^{-1}\delta(\theta)\exp(-z^2/d^2)H(t)\boldsymbol{e}_r. \tag{9}$$

Hence, from Eq. (8), the radial displacement of the particle on the outer surface is

$$u_r(b,\theta,z,t)=\sum_{nmk}\frac{\varepsilon[R^r_{nmk}(b,\xi_k,\omega_{nmk})]^2}{l\omega^2_{nmk}M_{nmk}}\cdot(1-\cos\omega_{nmk}t)\cdot\cos n\theta\cdot\cos\xi_k z, \tag{10a}$$

where ε is defined by

$$\varepsilon=\int_{-l}^{l}\exp(-z^2/d^2)\cos\xi_k z\,\mathrm{d}z. \tag{10b}$$

As the hollow cylinder is of infinite length, i.e. $l\to\infty$, interval between two successive roots $\Delta\xi_k=\pi/l$ approaches zero. Therefore, in the limit of l approaching infinity, the summation over the index k in Eq. (10a) will be replaced by the integral over the continuous eigen-value ξ

$$u_r(b,\theta,z,t)=\int_0^\infty\mathrm{d}\xi\sum_{n=0}^{\infty}\sum_{m=1}^{\infty}\frac{\varepsilon[R^r_{nm}(b,\xi,\omega_{nm})]^2}{\pi\omega^2_{nm}M_{nm}}\cdot(1-\cos\omega_{nm}t)\cdot\cos n\theta\cdot\cos\xi z, \tag{11a}$$

where

$$M_{nm}=\pi\int_a^b\rho[{R^r_{nmk}}^2+{R^\theta_{nmk}}^2+{R^z_{nmk}}^2]r\,\mathrm{d}r. \tag{11b}$$

For the ES, the surface force density can be written as

$$\boldsymbol{s}(r,\theta,z,t)\Big|_{r=b}=b^{-1}\delta(\theta)\exp(-z^2/d^2)\delta(t)\boldsymbol{e}_r. \tag{12}$$

In the limit of l approaching infinity, the radial displacement of the particle on the outer surface of a hollow cylinder is

$$u_r(b,\theta,z,t)=\int_0^\infty\mathrm{d}\xi\sum_{n=0}^{\infty}\sum_{m=1}^{\infty}\frac{\varepsilon[R^r_{nm}(b,\xi,\omega_{nm})]^2}{\pi\omega_{nm}M_{nm}}\cdot\sin\omega_{nm}t\cdot\cos n\theta\cdot\cos\xi z, \tag{13}$$

where ε and M_{nm} are the same as in Eq. 11(a). Indeed, Eq. (13) can be obtained by taking one-order derivative of Eq. (11a).

4 Numerical simulations

In our numerical simulations, all waveforms are received at the outer surface of a hollow cylinder and the geometry and material parameters are the thickness $h=5.5$ mm, OD = 88.7 mm, the spot radius $d=1.0$ mm, the Poisson's ratio $\gamma=0.28$, the Lamé constant $\mu=8.4$ GPa and the density $\rho=7.8\times10^3$ kg/m^3.

Figs. 3 and 4 show the radial displacements from two longitudinal type modes (L(0, 1) and L(0, 2)) and four flexural type modes (F(1, 1), F(1, 2), F(2, 1) and F(2, 2)) generated by the AS and the ES, respectively. The total radial displacements and their distributions of time-frequency analysis from all longitudinal and flexural type modes generated by the AS and the ES are indicated in Figs. 5 and 6 with the source-receiver distance $z=0.6$ m and propagating directions $\theta=0°$.

Figs. 3(a) and 4(a) have a common feature that is the early arrival ($t=110$ μs) of a relatively low-amplitude and lower frequency component because the L(0, 1) mode propagates at a large group velocity $C_g\approx C_p$ at lower frequency (see Fig. 2(a)). But Fig. 4(a) has a feature, which is distinct from that of Fig. 3(a). In Fig. 4(a), a sharp spike of very high frequency arrives at about 180 μs, which comes from higher frequency of the $L(0,1)$ mode propagating at a relatively large and unvarying group velocity, but Fig. 3(a) does not have this spike. The difference between Fig. 3(a) and Fig. 4(a) can be contributed to that the signal $\delta(t)$ has plenty of components of high frequency while the dominant components of signal $H(t)$ are components of low frequency. The same difference occurs between the modes F(n, 1) generated by the AS and those generated by the ES. The features of transient waveform from other modes can also be explained based on the dispersion curves and the frequency spectrum of the source.

The waveforms of L(0, 2) generated by the ES (Fig. 3(b)) and AS (Fig. 4(b)) have a common feature that a nearly constant frequency and large amplitude component was received after $t=360$ μs. But the former has a relatively high frequency component superposed in a low frequency component received between 200 μs~350 μs which could not be found in the latter.

The waveform of F(1, 1) generated by the ES (Fig. 4(c)) has two features. The first feature is that a spike was received about $t=180$ μs. The second feature is that a relatively low frequency component

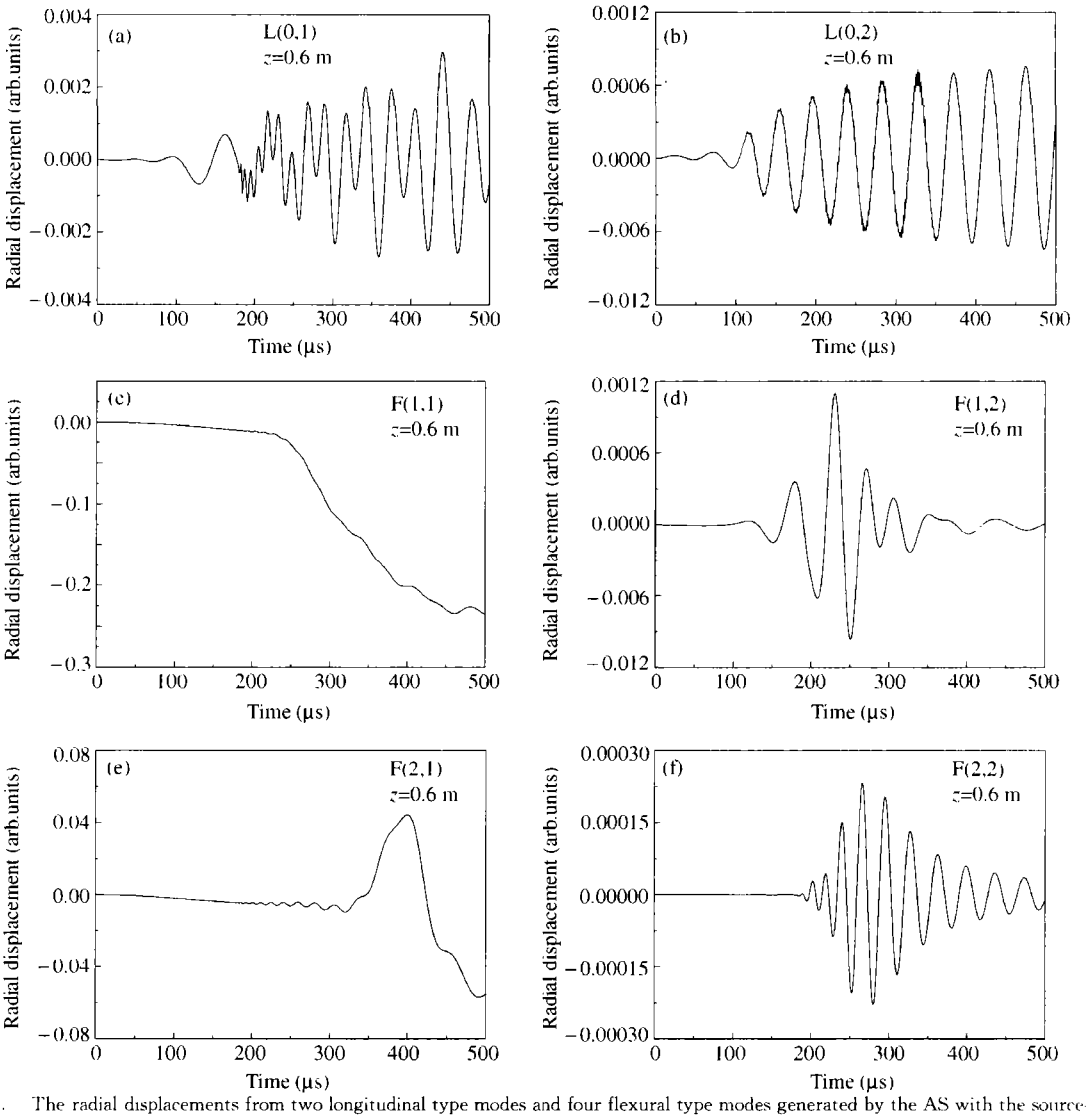

Fig. 3. The radial displacements from two longitudinal type modes and four flexural type modes generated by the AS with the source-receiver distance $z = 0.6$ m and the propagating direction $\theta = 0°$: (a) L(0,1); (b) L(0,2); (c) F(1,1); (d) F(1,2); (e) F(2,1); and (f) F(2,2).

superposed in a very low frequency and very large amplitude component was received after $t = 200$ μs. But only a very low frequency and very large amplitude component could be found in that generated by the AS (Fig. 3(c)). We can find the waveform of F(1,1) either generated by the ES or the AS has the largest amplitude among all guided wave modes which means that mode F(1,1) contributes most to the total energy.

The waveforms in Fig. 5(a) and Fig. 6(a) were analyzed using the STFT. A 0.256 ms Kaiser window was used in the computations of the STFT. The STFT images give the arrival time of each frequency component and, therefore, directly show the relationship between the group velocity and frequency. Importantly, we can observe the distributions of energy either among all modes or in the frequency domain qualitatively from the STFT images. Comparing Fig. 6(b) with Fig. 5(b), we can find that the attenuation of the high-order modes generated by the AS is far faster than that of the high-order modes generated by the ES. And the modes L(0,1) and F(n,1) have dominant energy, especially to the guided waves generated by the AS. The modes F(n,2) and F(n,4) could not be observed from all STFT images, because their energy is too small. From the STFT images, we also can easily find the total displacement generated by the ES has richer frequency components than that generated by the AS, and the former has higher frequency components than the latter.

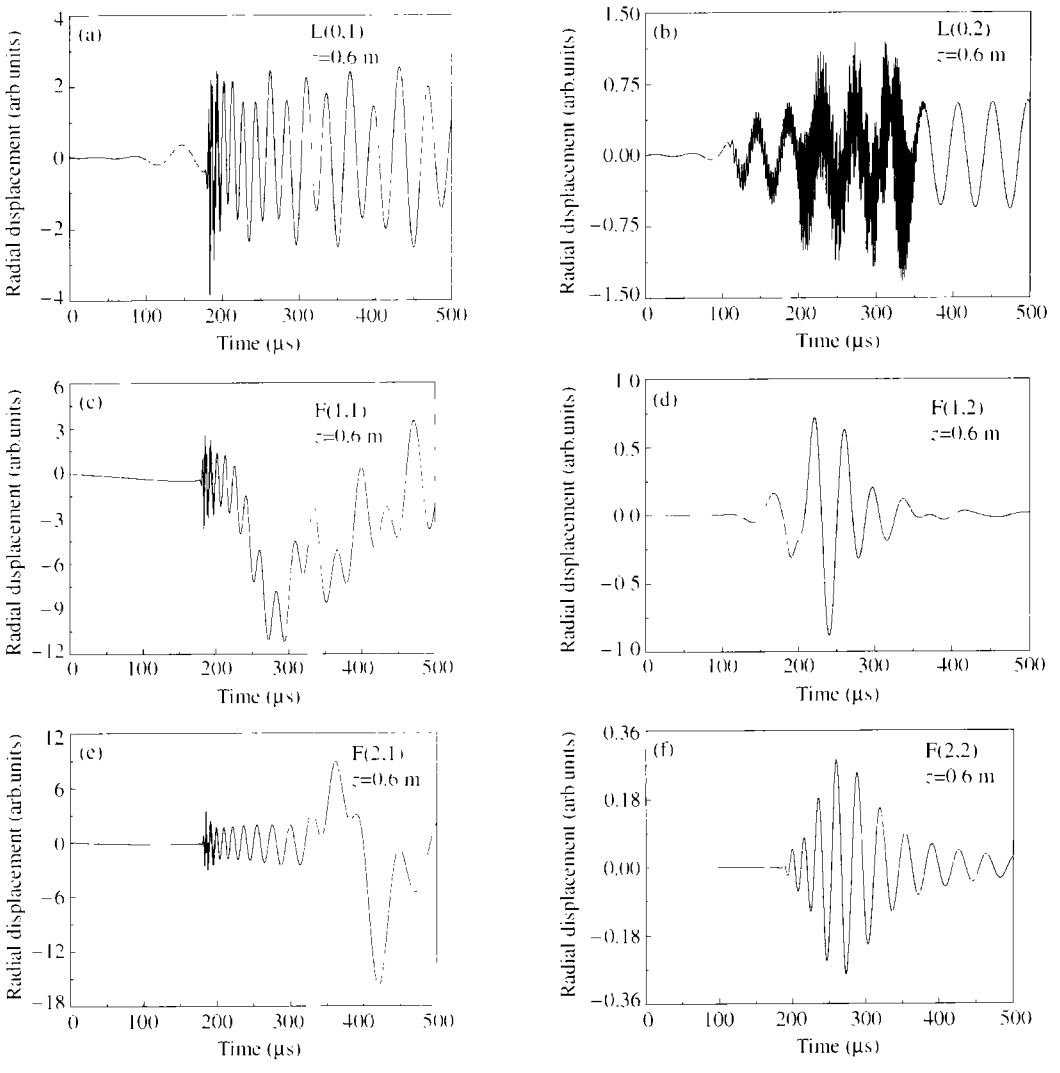

Fig. 4. The radial displacements from two longitudinal type modes and four flexural type modes generated by the ES with the source-receiver distance $z = 0.6$ cm and the propagating direction $\theta = 0°$: (a) L(0,1); (b) L(0,2); (c) F(1,1); (e) F(2,1); and (f) F(2,2).

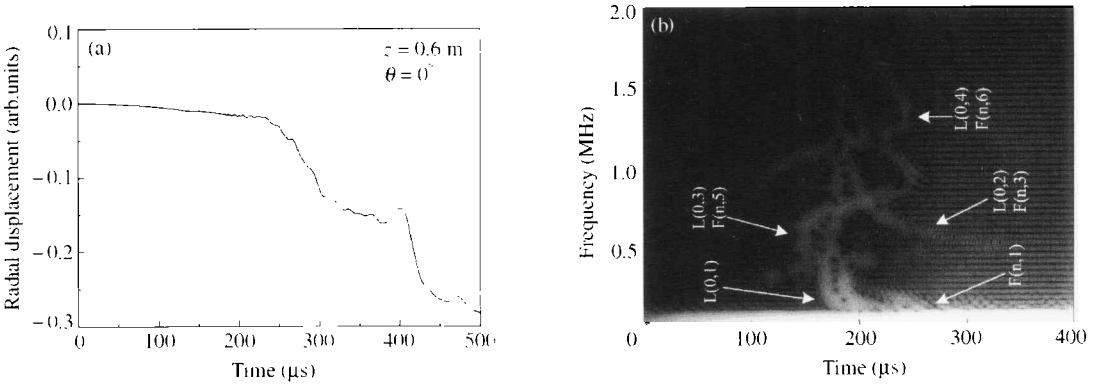

Fig. 5. Total radial displacements from all longitudinal and flexural type modes generated by the AS with the source-receiver distance $z = 0.6$ m and the propagating direction $\theta = 0°$ (a) and the corresponding distribution of time-frequency (b).

We give the transient waveforms of the mode F(3,1) received at four different points in Fig. 7, from which it is clearly seen that the amplitude of the displacement becomes smaller and the waveform expands along with the propagation of the guided waves because of the dispersion effects.

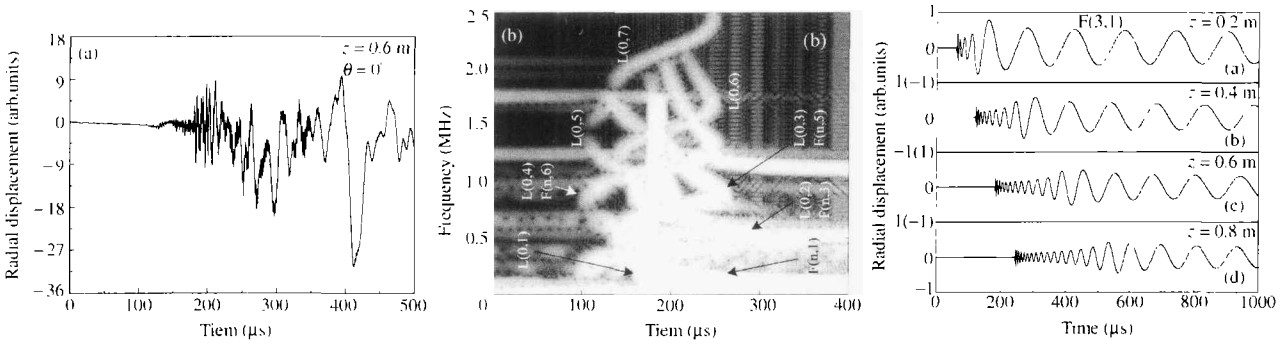

Fig. 6. Total radial displacements from all longitudinal and flexural type modes generated by the ES with the source-receiver distance $z = 0.6$ cm and the propagating direction $\theta = 0°$ (a); and the corresponding distribution of time-frequency (b).

Fig. 7. The waveforms of mode F(3, 1) generated by the ES with OD = 88.7 mm, $h = 5.5$ mm, $\theta = 0°$ and different source-receiver distance: (a) $z = 0.2$ m; (b) $z = 0.4$ m; (c) $z = 0.6$ m; (d) $z = 0.8$ m.

5 Conclusion

We have presented some numerical simulations of the guided waves generated by pulsed laser in hollow cylinders. Two types of acoustic source, the AS and the ES, have been discussed, respectively. The waveforms of total radial displacements were analyzed using the STFT. We find modes L(0, 1) and F(n, 1) have dominant energy among all guided modes generated by the laser pulse. The total displacements generated by the ES have richer frequency components than that generated by the AS. And the dispersion effects have been observed by calculating the displacements of mode F(3, 1) with four different source-receiver distances.

References

1 Silk, M. G. et al. The propagation in metal tubing of ultrasonic wave modes equivalent to lamb waves. Ultrasonics, 1979, 17: 11.

2 Alleyne, D. N. et al. The reflection of guided waves from circumferential notchss in pipes. J. Appl. Mech, 1998, 65(3): 635.

3 Lowe, M. J. S. et al. The mode conversion of a guided wave by a part-circumferential notch in a pipe. J Appl. Mech., 1998, 65(3): 649.

4 Ditri, J. J. et al. Excitation of guided elastic wave modes in hollow cylinders by applied surface tractions. J. Appl. Phys., 1992, 72(7): 2589.

5 Shin, H. J. et al. Guided waves by axisymmetric and non-axisymmetric surface loading on hollow cylinders. Ultrasonics, 1999, 37: 355.

6 Li, J. Excitation and propagation of non-axisymmetric guided waves in a hollow cylinder. J. Acoust. Soc. Am., 2001, 109(2): 457.

7 Rose, J. L. et al. Ultrasonic guided wave flexural mode tuning for limited access pipe inspection. Review of Progress in Quantitative Nondestructive Evaluation, 2001, 20A:164.

8 Tang, L. G. et al Theoretical investigation of the laser-generated guided waves in hollow cylinders. Acta Acustica (in Chinese), 2001, 26: 489.

9 Gazis, D. C. Three-dimensional investigation of the propagation of waves in hollow circular cylinders I. Analytical foundation. J. Acoust. Soc. Am., 1959, 31(5): 568.

10 Frost, H. M. Electromagnetic-ultrasonic transducer: principles, practice and applications. In: Physical Acoustics XIV. New York: Academic Press, 1979, 179－275.

11 Dobbs, E. R. Electromagnetic generation of ultrasonic waves. In: Physical Acoustics X. New York: Academic Press, 1973, 127－189.

12 Hutchins, D. A. et al. Laser generated ultrasound at modified metal surfaces. Ultrasonics, 1981, 19: 103.

13 Hutchins, D. A. et al. Laser generation as a standard acoustic source in metals. Appl. Phys. Lett., 1981, 38(9): 677.

14 Weaver, R. L. et al. Axisymmetric elastic waves excited by a point source in a plate. J. Appl. Mech., 1982, 49: 821.

15 Meitzler, A. H. Mode coupling occurring in the propagation of elastic pulses in wires. J. Acoust. Soc. Am., 1961, 33(4): 435.

16 Zemanek, J. An experimental and theoretical investigation of elastic wave propagation in a cylinder. J. Acoust. Soc. Am., 1972, 51(1): 265.

17 Eringen, A. C. et al. Elastodynamics, Vol. 2. New York: Academic Press, 1975, 111－117.

18 Cheng, J. C. et al Excitation of thermoelastic waves in plates by a pulsed laser. Appl. Phys., 1995, A61: 311.

19 Cheng, J C. et al Quantitative theory for laser-generated Lamb waves in orthotropic thin plates. Appl. Phys Lett., 1999, 74(14): 2087.